

Laser-induced plasma cloud interaction and ice multiplication under cirrus cloud conditions

Thomas Leisner^{a,b,1}, Denis Duft^a, Ottmar Möhler^a, Harald Saathoff^a, Martin Schnaiter^a, Stefano Henin^c, Kamil Stelmazczyk^d, Massimo Petrarca^c, Raphaëlle Delagrange^c, Zuoqiang Hao^d, Johannes Lüder^d, Yannick Petit^c, Philipp Rohwetter^d, Jérôme Kasparian^c, Jean-Pierre Wolf^c, and Ludger Wöste^d

^aInstitute for Meteorology and Climate Research, Karlsruhe Institute of Technology, 76021 Karlsruhe, Germany; ^bInstitut für Umweltphysik, Universität Heidelberg, 69120 Heidelberg, Germany; ^cGroup of Applied Physics, Université de Genève, CH-1211 Genève 4, Switzerland; and ^dInstitut für Experimentalphysik, Freie Universität Berlin, 14195 Berlin, Germany

Edited by A. R. Ravishankara, National Oceanic and Atmospheric Administration Earth System Research Laboratory, Chemical Sciences Division, Boulder, CO, and approved May 7, 2013 (received for review December 19, 2012)

Potential impacts of lightning-induced plasma on cloud ice formation and precipitation have been a subject of debate for decades. Here, we report on the interaction of laser-generated plasma channels with water and ice clouds observed in a large cloud simulation chamber. Under the conditions of a typical storm cloud, in which ice and supercooled water coexist, no direct influence of the plasma channels on ice formation or precipitation processes could be detected. Under conditions typical for thin cirrus ice clouds, however, the plasma channels induced a surprisingly strong effect of ice multiplication. Within a few minutes, the laser action led to a strong enhancement of the total ice particle number density in the chamber by up to a factor of 100, even though only a 10^{-9} fraction of the chamber volume was exposed to the plasma channels. The newly formed ice particles quickly reduced the water vapor pressure to ice saturation, thereby increasing the cloud optical thickness by up to three orders of magnitude. A model relying on the complete vaporization of ice particles in the laser filament and the condensation of the resulting water vapor on plasma ions reproduces our experimental findings. This surprising effect might open new perspectives for remote sensing of water vapor and ice in the upper troposphere.

nonlinear optics | secondary ice | lightning

Clouds and their feedbacks in the climate system are the largest source of uncertainty in our ability to predict future climate (1). At the same time, they play an important role in the atmospheric part of the fresh water cycle. In both cases, cloud ice formation is of central importance.

Cirrus clouds are formed over large areas of the upper troposphere at altitudes between 6 and 12 km at temperatures below -37°C (2) where only ice can exist as all water freezes by homogeneous nucleation (3). They cool the earth surface by reflecting incoming solar radiation and at the same time warm it by absorbing outgoing thermal radiation. Although, on average, the warming effect seems to prevail, the magnitude and sign of the net climatic effect of cirrus clouds depend on the height and temperature of the cirrus cloud as well as on the size distribution and shape of the ice crystals (4). In contrast to liquid phase clouds, the nucleation of ice clouds is often kinetically hindered, so that large areas of supersaturation with respect to ice seem common especially in the upper tropical troposphere (5). Relative humidity and saturation is difficult to measure at these low temperatures, however, both by in situ measurements and by remote sensing.

Precipitation in midlatitude clouds is predominantly initiated via the Wegener–Bergeron–Findeisen process (6), which relies on the heterogeneous freezing of supercooled cloud droplets promoted by ice-active aerosol particles and the subsequent growth of the ice particles by water vapor deposition and riming. As good ice nuclei are very rare in the atmosphere (7), ice and liquid cloud particles can coexist at temperatures above -37°C

and artificial seeding of clouds with ice-active substances as silver iodide or dry ice may be used to trigger precipitation. Moreover, lightning formation in mixed-phase clouds seems to be related to the interaction between liquid and solid phase particles in clouds, although the details of cloud electrification are still under debate. Lightning discharges themselves have long been speculated to modify cloud ice formation and thereby precipitation (8), as they have been reported to amplify radar echoes from ice particles in thunderclouds and initiate localized rain gushes (9). So far, no conclusive mechanism for these effects has been found yet. Early laboratory experiments on the effects of electrical discharges on supercooled and mixed-phase clouds have been plagued by contamination from the aerosol generated by the discharges from the electrode material. As such discharges can now be produced or initiated electrode free by high-power ultrashort laser pulses, we have investigated the interaction of laser plasma channels with water and ice clouds in the large cloud simulation chamber Aerosol Interaction and Dynamics in the Atmosphere (AIDA).

High-power lasers allow producing plasma channels in the atmosphere by nonlinear optical effects leading to filamentation. Light filaments (10–14) constitute a nonlinear, self-guided propagation mode of ultrashort laser pulses above a critical power of 3–6 GW in air for 800-nm radiation. They carry a typical intensity as high as $5 \times 10^{13} \text{ W/cm}^2$, allowing to ionize and photooxidize (15) the air at kilometer-range distances (16), leaving a plasma trail behind them. Their ability to propagate unperturbed in adverse conditions like turbulence (17) or clouds (18) designs them for atmospheric applications (10, 13).

In this contribution, we investigate the ability of such laser-induced plasma channels to influence and modify both mixed-phase and ice clouds produced in a large aerosol and cloud chamber (19) using a mobile terawatt laser system (20).

Results

Laser filament–cloud interaction experiments have been performed over a range of tropospheric conditions with temperatures between 10°C and -60°C , and pressures from 0.6 to 1 bar. Clouds were created by adiabatic expansion in atmospheres consisting of synthetic air with cloud condensation nuclei (CCN) either produced photochemically by the laser filament action (21) or introduced before the expansion as well-defined mineral dust and sulfuric acid particles (for details, see *Methods*). Laser filaments were applied intermittently, either before the

Author contributions: T.L., O.M., H.S., K.S., J.K., J.-P.W., and L.W. designed research; T.L., O.M., H.S., M.S., S.H., K.S., M.P., R.D., Z.H., J.L., Y.P., P.R., and J.K. performed research; T.L., D.D., O.M., H.S., M.S., J.K., and J.-P.W. analyzed data; and T.L., D.D., J.K., and J.-P.W. wrote the paper.

The authors declare no conflict of interest.

This article is a PNAS Direct Submission.

¹To whom correspondence should be addressed. E-mail: thomas.leisner@kit.edu.

expansion, during the dry part of the expansion, or during the cloud condensation phase.

Our results do strongly depend on the temperature of the cloud under investigation. At temperatures above the limit of homogeneous freezing, the filaments did not modify the activation of preexisting aerosol particles to liquid cloud droplets, which, within our limits of experimental uncertainty, always occurred at water saturation. Aerosol particles generated photochemically by the laser plasma before the expansion (21) were equally active as cloud condensation nuclei. Upon further cooling, cloud droplets that had nucleated on these aerosols froze homogeneously as soon as the relative humidity reached the Koop limit for homogeneous freezing (22), indicating they are at least partially soluble and that any insoluble part, if present, is not active as a heterogeneous ice nucleus. When the laser filaments were produced within a cloud of supercooled water droplets, they did not induce ice formation even at the lowest temperatures above the limit of homogeneous freezing. If at those temperatures pure ice clouds were produced by deposition nucleation of ice on mineral dust particles, the laser filaments did not have any discernible effect. These findings contradict a direct ice-nucleating effect of plasma discharges in supercooled droplets and do not provide evidence for ice nucleation in the acoustic shockwave created by the laser plasma itself or by its interaction with the cloud droplets or ice crystals. Although the shockwaves created in our experiment (23) may have similar amplitudes to shockwaves created by natural lightning, they are of much shorter duration.

The situation changes profoundly when the laser filaments interact with ice clouds at temperatures below the limit of homogeneous freezing and at supersaturation with respect to ice. Under these conditions, we observe the laser-induced production of a large number of additional ice particles. The laser filaments continue to produce ice particles until the relative humidity with respect to ice (RH_i) is brought back to values very close to unity. The effect is illustrated in Fig. 1, where cirrus cloud-type expansions with and without laser filament action are compared. Without laser action, ice forms by deposition mode nucleation on mineral dust particles as soon as RH_i reaches 1.1 (visible by a few optical detector counts in Fig. 1D). These initial ice particles are formed at a concentration of less than 1 cm^{-3} and grow to sizes up to a diameter of $50 \text{ }\mu\text{m}$, thereby hardly depleting the ice supersaturation (Fig. 1B).

If laser filaments are produced, an additional mode of ice appears about 1 min after the formation of the first ice particles. This laser-induced ice generation is apparent from a steep and roughly exponential increase in the backward and forward light-scattering intensities and is clearly detected in the optical particle counter (OPC) as well (Fig. 1D). The high number of laser-generated ice particles rapidly reduces the ice supersaturation (Fig. 1B). The dashed area between the two RH_i curves of Fig. 1B visualizes the amount of water vapor converted into ice as a result of the laser action. After a few minutes, RH_i has dropped to unity and the secondary ice generation terminates.

For the following discussion we will refer to this surprising effect of the laser filaments as “filament-induced secondary ice multiplication” (FISIM). This term is justified further by a more detailed analysis of the ice formation kinetics below.

A total of 39 similar experiments with natural and artificial heterogeneous ice nuclei or with homogeneously frozen ice particles present has been conducted over a broad range of temperature and relative humidity. FISIM eventually enhanced the total ice particle number density in the AIDA chamber by up to a factor of 100, even though only a fraction of 10^{-9} of the AIDA volume was exposed to the laser filaments produced at a repetition rate of 10 Hz for a period of a few minutes. The effect was only observed however, if the following three conditions were all met: (i) The temperature is below $-37 \text{ }^\circ\text{C}$, which

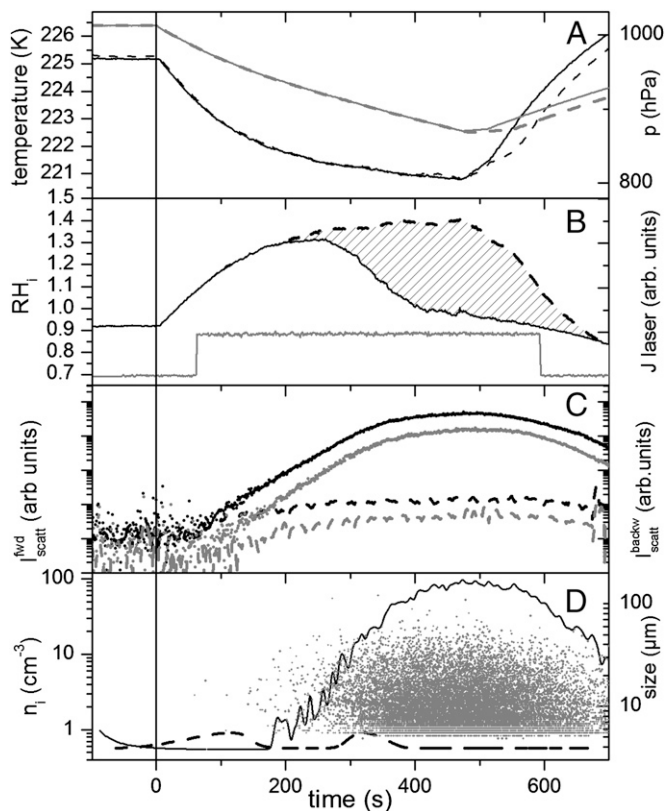


Fig. 1. Typical expansion profile and ice cloud characteristics at low temperatures, with (solid lines) and without (dashed lines) filament action. The black and gray curves correspond to left and right vertical axes, respectively. (A) Chamber gas phase temperature and pressure. (B) Relative humidity with respect to ice and duration of laser operation. (C) Forward and backward light-scattering intensity. (D) Ice particle number concentration and ice particle size distribution given only for the case with laser action.

is the limit of homogeneous freezing of pure water droplets. (ii) The relative humidity with respect to ice is above unity so that ice particles can grow. (iii) Preexisting ice particles are present. The ice number density of preexisting ice particles required to trigger the effect is very low; an initial ice number concentration below 0.2 cm^{-3} (~ 0.02 particle in the filament volume at each laser pulse) was sufficient. Laser filaments alone, without any ice particles being present, were not efficient in producing new ice particles even at RH_i as high as 130%.

The second condition is illustrated in an experiment conducted around a temperature of $-50 \text{ }^\circ\text{C}$, where two phases of laser action and pumping were used (Fig. 2). In this case, a thin ice cloud ($c_{\text{ice}} = 2 \text{ cm}^{-3}$) was nucleated heterogeneously on mineral dust particles around time $t = 100 \text{ s}$. The laser was fired at $t = 400 \text{ s}$ when the initially nucleated ice particles were grown to an optical diameter of about $50 \text{ }\mu\text{m}$. Within less than 100 s, the laser filaments led to the production of a large number of small ice particles with the ice number density reaching about 50 cm^{-3} at $t = 700 \text{ s}$. At that time, the laser action was stopped as RH_i had dropped to unity and no further ice was produced. At $t = 750 \text{ s}$, pumping was stopped and the ice cloud started to evaporate at a relative humidity level slightly below unity. At $t = 1,450 \text{ s}$, the laser was fired again into the evaporating ice cloud for a second period but with no detectable effect. Only after pumping was resumed at $t = 1,630 \text{ s}$, a second mode of laser-generated ice particles could be observed as soon as RH_i increased above unity again. The laser-generated additional ice particles are easily discerned from typical ice particles formed in AIDA as a result

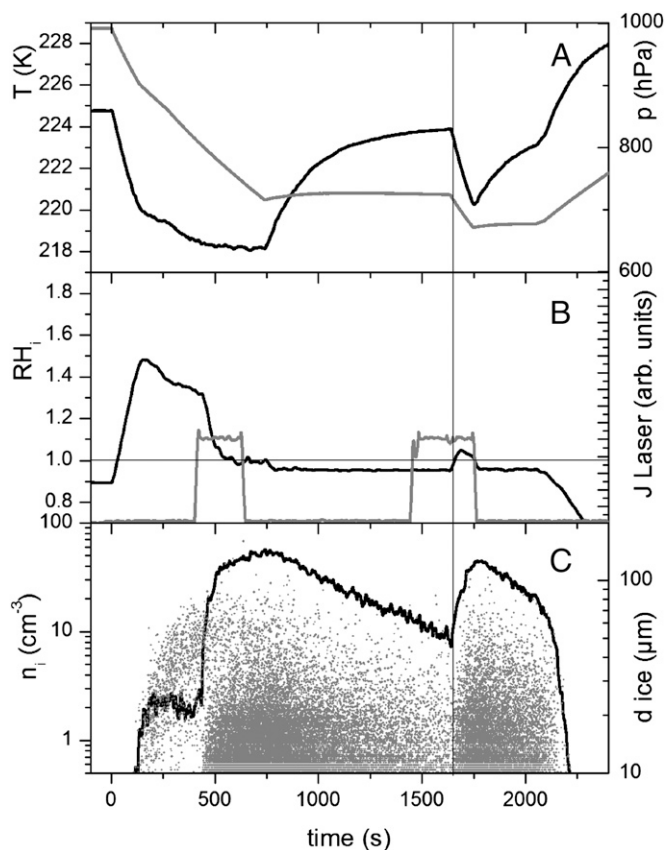


Fig. 2. Typical expansion profile and ice cloud characteristics at low temperatures and two periods of laser action. The black and gray curves correspond to the left and right vertical axes, respectively. (A) Chamber gas phase temperature and pressure. (B) Relative humidity with respect to ice and duration of laser operation. (C) Forward and backward light-scattering intensity. (D) Ice particle number concentration and ice particle size.

of heterogeneous nucleation as they are considerably smaller than the preexisting ice crystals: Their size distribution ranges from the submicrometer regime up to about 30 μm , compared with $\sim 50 \mu\text{m}$ for the preexisting ones (Fig. 2C).

Discussion

The need for preexisting ice particles to observe FISIM implies that the interaction of laser filaments with ice particles plays a central role in the ice multiplication process. For typical laser parameters used in our experiments and at typical initial ice number concentrations, only about 1 of 10–100 laser pulses interacts with an ice particle within the 80 mm^3 of the filament volume. Even in a dense ice cloud (50 cm^{-3}), only a few ice particles are found within the volume of the filaments during each laser pulse. The fast growth of the ice particle number density implies that each laser–ice particle interaction produces an extremely large number of secondary ice particles with a size limited to the nanometer range by water mass conservation. Their subsequent optical detection indicates that they can grow into the μm size range while being distributed through the ice-supersaturated AIDA atmosphere. Eventually, they are transported back into the filament region where they can contribute anew to the ice multiplication process. The secondary ice particles could be created either by laser-induced mechanical shattering of the preexisting ice particles or by thermal evaporation of the ice particles and a subsequent condensation of the water vapor to form a large number of small droplets. However, shattering and subsequent growth of the fragments should be effective at temperatures

above the threshold of homogeneous freezing as well. We therefore conclude that we observe the condensation and subsequent freezing of liquid water, i.e., condensation freezing. The latter requires both water supersaturation and a temperature below the limit of homogeneous freezing and leads to the following mechanism for FISIM: The laser filaments deposit a considerable amount of electronic excitation energy in the preexisting ice particles by nonlinear interactions. This amount of energy is sufficient to completely evaporate the ice particles, even if they are hit only partially. On a millisecond timescale, the resulting water vapor plume expands and cools down by molecular or turbulent diffusional mixing with the surrounding cold gas. Due to the strongly nonlinear dependence of water vapor pressure on temperature, this leads to a zone of supersaturation similar to the situation in a diffusion condensation chamber.

Throughout this zone, water vapor will condense either on preexisting aerosol particles or on the ions remaining from the laser plasma at a relative humidity above the threshold for ion induced nucleation of $\text{RH}_w = 4$ (24, 25), or homogeneously around $\text{RH}_w = 15$ (26). A simple diffusion–mixing calculation shows that very high supersaturation with respect to water can be reached in a large volume around the interaction region (e.g., $\text{RH}_w > 4$ in a volume of 1 cm^3 and $\text{RH}_w > 15$ in a volume of 0.5 cm^3 for an initial spherical ice crystal of 80- μm diameter) (Methods). The nucleated nanodroplets may freeze and survive as tiny ice crystals provided the temperature lies below -37°C . These ice crystals are then rapidly dispersed throughout the

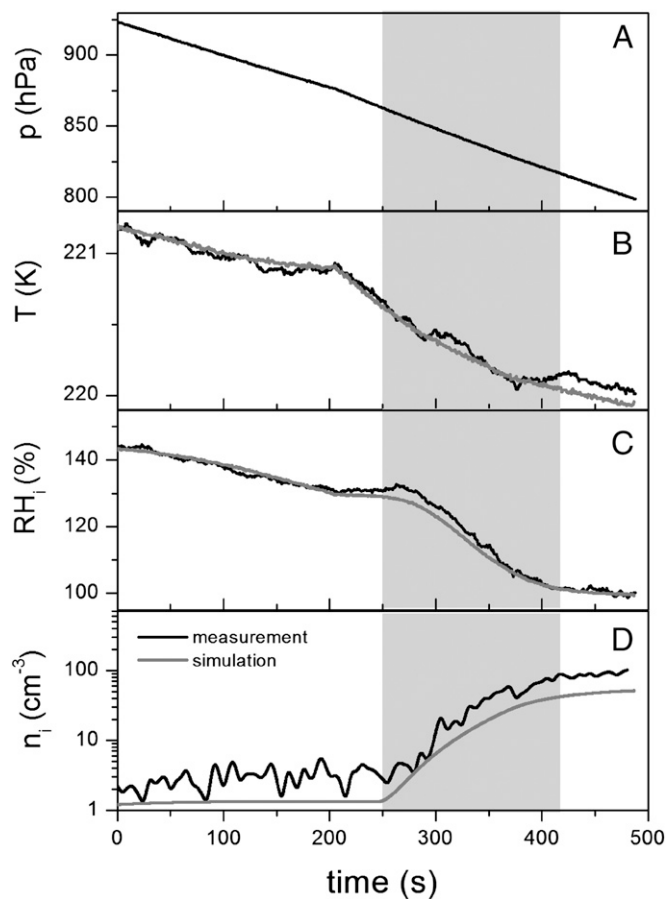


Fig. 3. Measured (black) and modeled (gray) expansion and ice cloud parameters. (A) Pressure, the model is driven with the experimental pressure trace. (B) Temperature. (C) Relative humidity with respect to ice. (D) Ice crystal number density. The period of laser plasma action is shaded gray.

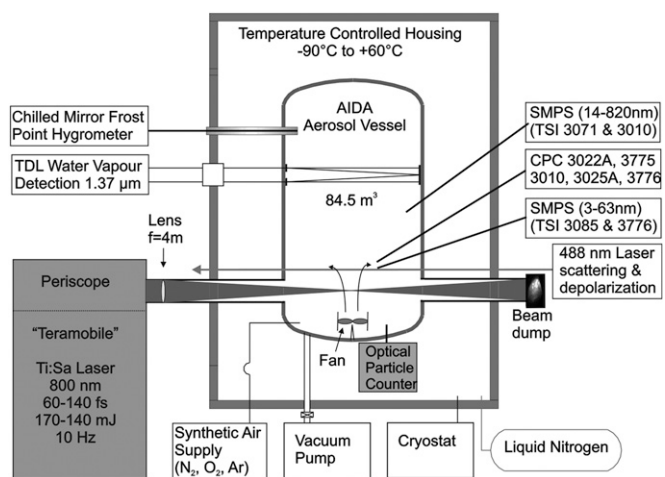


Fig. 4. Schematic of the experimental setup of the Teramobile laser system at the AIDA aerosol and cloud chamber. The terawatt laser beam is generated in a container outside the AIDA hall and directed via transfer optics, a focusing lens ($f = 4$ m), and an entrance window (139-mm diameter, 9.8-mm thickness) across the AIDA vessel and across the air flux from its mixing fan. The beam exits at the opposite side through an exit window into a beam dump.

chamber by the mixing fan and grow subsequently into the micrometer-size regime if the chamber supersaturation with respect to ice is above unity.

To test this mechanism, we implemented it in a kinetic model (for details, see *Methods*) that quantitatively describes the number density and size distribution of the secondary ice produced by the laser filaments. It relies only on the measured pressure drop curve $p(t)$ and the observed volume of the laser filaments as inputs. The initial number density and size distribution of ice particles in the chamber are adapted to reproduce the experimentally observed relative humidity curve before the laser filament action and coincide well with the measured ice particle number density during that period. The only remaining parameter in the model, the number concentration of cloud nuclei ρ_{cn} that are available for the condensation of water around the plasma-evaporated ice crystals, is used as a free fitting parameter. The model provides the time-dependent averaged gas phase temperature, relative humidity, ice number concentration, and ice particle size distribution. Even though a time-independent ion concentration is used and details of the fluid and aerosol dynamics in the filament plasma and in the fan vented simulation chamber are ignored, the model fitted the experiments well with the only adjustable parameter ρ_{cn} ranging between $8 \times 10^8 \text{ cm}^{-3}$ to $2.5 \times 10^9 \text{ cm}^{-3}$. As an example, a comparison between the measured quantities and the model output is given in Fig. 3. The high values obtained for ρ_{cn} exclude preexisting aerosol particles as condensation nuclei but are consistent with homogeneous nucleation or possibly ion-induced nucleation. Highest supersaturation around the evaporated ice crystals is reached after about 1 ms after the plasma was ignited. Within that period, the initial ion density in the plasma filaments of about 10^{16} cm^{-3} has decayed almost completely due to recombination between electrons and positive ions (27). A few negative and positive charges will have survived by electron attachment to molecules, however. Subsequently formed molecular aggregates with a strongly reduced mobility may then act as condensation nuclei. Even though we are not able to distinguish between charge-induced and homogeneous nucleation, the overall very good agreement of the model with the experimental results strongly supports the proposed FISIM mechanism.

Conclusion and Outlook

We have observed the interaction of laser filaments with water and ice clouds in a large simulation chamber. Although the laser had virtually no effect in interacting with liquid phase clouds and mixed-phase clouds above the temperature of homogeneous freezing, it profoundly modified the microphysics and optical properties of cirrus clouds under the conditions of ice supersaturation. The laser created a large amount of secondary ice particles that quickly exceeded the number concentration of initial ice particles by a factor of 100 in a volume nine orders of magnitude larger than the filament volume itself. Under conditions representative for ice-supersaturated regions in the upper troposphere, each individual laser pulse produced several millions of new ice particles that grew to sizes of a few tens of micrometers in diameter and are thus easily detected optically. This effect could be exploited to measure remotely the ice supersaturation in the upper troposphere, a quantity that is very difficult to assess otherwise and has given rise to some scientific controversy due to its importance for the radiative budget of the earth (28). The large ice multiplication factor described here might open the possibility for laser modification of natural cirrus clouds or the artificial seeding of cirrus clouds in ice-supersaturated regions. The main effect would be to create cirrus clouds that contain more but smaller ice particles, which might resemble laser written contrails. Due to the reduced gravitational settling, such clouds might live longer than unperturbed clouds.

In mixed-phase clouds warmer than $-37 \text{ }^\circ\text{C}$, laser filament-produced plasma channels had no discernible influence on cloud activation or ice formation. This discourages direct ice nucleation following lightning strokes but does not rule out more indirect effects like increased scavenging rates of ice nuclei by electrified cloud droplets, which are beyond the scope of this study.

Methods

An overview of the experimental setup and the main instrumentation is given in Fig. 4. It relies on the Teramobile laser system illuminating the atmosphere inside the AIDA aerosol and cloud chamber featuring 4-m diameter and 7.5-m height (84.5 m^3). The laser emitted 170-mJ, 60-fs pulses centered at 800 nm, at a repetition rate of 10 Hz. Its beam was expanded to 10-cm diameter and focused by an $f = 4$ m lens into the center of the cloud chamber, in the center of which it generated a bunch of typically 20 filaments of 50-cm length, covering a total volume of 80 mm^3 , which corresponds to a 10^{-9} fraction of the total chamber volume.

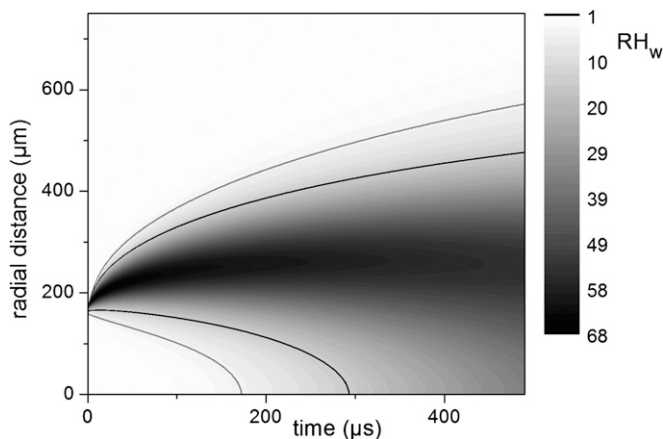


Fig. 5. The spatiotemporal profile of the relative humidity with respect to water around a laser-evaporated ice particle assuming pure diffusional mixing. Time $t = 0$ corresponds to a water vapor sphere from a spherical ice particle of an initial diameter of $15 \text{ } \mu\text{m}$. Isolines corresponding to $\text{RH}_w = 4$ (gray) and $\text{RH}_w = 15$ (black) are shown.

Experiments have been performed over a range of tropospheric conditions with temperatures between 10 °C and –60 °C, and pressures from 0.6 to 1 bar. Clouds were created by adiabatic expansion in atmospheres consisting of synthetic air [99.998% purity, low hydrocarbon grade (Basi)]. CCN were either produced photochemically by the laser filament action or introduced before the expansion as well-defined mineral dust and sulfuric acid particles. A typical expansion rate was 8 mbar/min corresponding to an atmospheric updraft velocity of about 1 m/s. The chamber atmosphere was homogenized by a powerful mixing fan placed below the filaments throughout the experiments. The gas velocity at the mixing fan reached ~2 m/s, and the volume flow is about 200 L/s. Aerosol particles in the chamber were sampled through stainless-steel tubes placed ~15 cm above the laser filaments. Their number concentration was measured with condensation particle counters (CPCs) (3010, 3775, 3776; TSI) for particles larger than about 10, 4, and 2.5 nm, respectively, with a time resolution of 1 s. Aerosol particle size distributions (14–820 nm) were measured by using a scanning mobility particle sizer (DMA 3071 and CPC 3010; TSI) with a time resolution of 300 s. CCN particles and cloud hydrometeors were characterized by optical scattering measurements at 488 nm, both in the forward (2°) and backward (178°) directions, including a depolarization channel bearing information about the asphericity of the particles, distinguishing between liquid droplets and ice. Cloud hydrometeors were counted and individually sized by two OPCs (type welas2000; Palas) in the size ranges of 0.7–40 μm (OPC1) and 5–240 μm (OPC2). The phase and shape of the ice crystals were further analyzed by a small ice detector probe (SID 3; University of Hertfordshire, Hertfordshire, UK). Water vapor concentrations were measured in situ by a tunable diode laser spectrometer (29). Total water content was measured by a second tunable diode laser spectrometer and a dew point mirror (373LX; MBW) operating on heated sampling lines.

Our numerical model of the FISM process is based on a laser pulse by laser pulse tracking of the number density and mass of the ice particles in the cloud chamber. From this information, the ice particle number and ice mass within the laser filaments is calculated for every laser pulse. Assuming a complete evaporation of any ice particle hit by the laser filaments, the maximum extend of the volume supersaturated with respect to ion-induced water nucleation ($RH_w = 4$) is calculated for each evaporated ice particle. Even if a much higher supersaturation typical for homogeneous nucleation was required, the results would differ only slightly. This is illustrated in Fig. 5, where the temporal and spatial development of the zone of supersaturation

around a completely evaporated ice crystal in the absence of any condensation is shown. The gray line and the black line, indicating a supersaturation of $RH_w = 4$ and of $RH_w = 15$, respectively, enclose a volume that differs by less than a factor of 2.

The water vapor mass exceeding saturation is then distributed evenly among all nuclei in the supersaturated volume, which are assumed to be present at a constant number density ρ_{cn} . The resulting monodisperse ice particles (typical diameter, 10 nm) are assumed to be dispersed throughout the AIDA chamber by the action of the mixing fan and their diffusional growth in the time period up to the next laser pulse is calculated, resulting in a decrease of the relative humidity within the chamber. This procedure is repeated for every individual laser pulse, creating new secondary ice particles at the repetition rate of the laser. For each set of ice particles created from each laser pulse, the number and mass density is recorded and their subsequent growth is treated separately. Due to the growth of the earlier ice particles, ice particles produced at later times are created in a less humid cloud chamber and reach smaller sizes. This explains the experimentally observed broad size distribution of the secondary ice particles. In the model, all secondary ice particles are allowed to interact again with the laser and to produce higher generations of ice particles; this process proves to be effective only after the ice particles have grown to considerable size, however. The model is initialized using the measured chamber pressure, temperature, and relative humidity well in advance of the laser filament action and is driven by the measured pressure profile during the adiabatic expansion. The initial ice crystal number density and size is adapted to reproduce the measured relative humidity and temperature curve in the period before the filament action. The condensation nuclei density, ρ_{cn} , remains the only free parameter in the model that is used to fit the results.

ACKNOWLEDGMENTS. We are pleased to thank the AIDA team for their support of the measurement campaign. This work was supported by Deutsche Forschungsgemeinschaft, the Swiss National Science Foundation through the National Centre of Competence in Research Molecular Ultrafast Science and Technology program, and EUROCHAMP-2 (Integration of European Simulation Chambers for Investigating Atmospheric Processes), a research project within the European Commission Seventh Framework Programme (Grant E2-2010-04-20-0031). J.-P.W. acknowledges financial support from the European Research Council advanced grant “FilAtmo.”

- Intergovernmental Panel on Climate Change (2007) Climate change 2007: The physical science basis. *Contribution of Working Group I to the Fourth Assessment Report of the Intergovernmental Panel on Climate Change*, eds Solomon SD, et al. (Cambridge University Press, Cambridge and New York).
- Wang PH, Minnis P, McCormick MP, Kent GS, Skeens KM (1996) A 6-year climatology of cloud occurrence frequency from stratospheric aerosol and gas experiment II observations (1985–1990). *J Geophys Res* 101(D23):29407–29429.
- Stöckel P, Weidinger IM, Baumgärtel H, Leisner T (2005) Rates of homogeneous ice nucleation in levitated H₂O and D₂O droplets. *J Phys Chem A* 109(11):2540–2546.
- Liou KN (1986) Influence of cirrus clouds on weather and climate processes—a global perspective. *Mon Weather Rev* 114(6):1167–1199.
- Spichtinger P, Gierens K, Read W (2003) The global distribution of ice-supersaturated regions as seen by the Microwave Limb Sounder. *Q J R Meteorol Soc* 129(595):3391–3410.
- Pruppacher HR, Klett JD (1997) *Microphysics of Clouds and Precipitation* (Kluwer Academic, Dordrecht), 2nd revised and enlarged edition.
- DeMott PJ, et al. (2011) Resurgence in ice nuclei measurement research. *Bull Am Meteorol Soc* 92(12):1623–1635.
- Barker E, Bicknell JA, Griffiths RF, Latham J, Verma TS (1983) The scavenging of particles by electrified drops: Radar echo intensification following lightning. *Q J R Meteorol Soc* 109(461):631–644.
- Moore CB, Vonnegut B, Vrablik EA, McCaig DA (1964) Gushes of rain and hail after lightning. *J Atmos Sci* 21(6):646–665.
- Kasparian J, et al. (2003) White-light filaments for atmospheric analysis. *Science* 301(5629):61–64.
- Couairon A, Mysyrowicz A (2007) Femtosecond filamentation in transparent media. *Phys Rep* 441(2–4):47–189.
- Berge L, Skupin S, Nuter R, Kasparian J, Wolf JP (2007) Ultrashort filaments of light in weakly ionized, optically transparent media. *Rep Prog Phys* 70(10):1633–1713.
- Kasparian J, Wolf J-P (2008) Physics and applications of atmospheric nonlinear optics and filamentation. *Opt Express* 16(1):466–493.
- Chin SL, et al. (2005) The propagation of powerful femtosecond laser pulses in optical media: Physics, applications, and new challenges. *Can J Phys* 83(9):863–905.
- Petit Y, Henin S, Kasparian J, Wolf J-P (2010) Production of ozone and nitrogen oxides by laser filamentation. *Appl Phys Lett* 97(2):021108.
- Rodriguez M, et al. (2004) Kilometer-range nonlinear propagation of femtosecond laser pulses. *Phys Rev E Stat Nonlin Soft Matter Phys* 69(3 Pt 2):036607.
- Salame R, et al. (2007) Propagation of laser filaments through an extended turbulent region. *Appl Phys Lett* 91(17):171106.
- Courvoisier F, et al. (2003) Ultraintense light filaments transmitted through clouds. *Appl Phys Lett* 83(2):213–215.
- Wagner R, et al. (2009) A review of optical measurements at the aerosol and cloud chamber AIDA. *J Quant Spectrosc Radiat Transf* 110(11):930–949.
- Wille H, et al. (2002) Teramobile: A mobile femtosecond-terawatt laser and detection system. *Eur Phys J Appl Phys* 20(3):183–190.
- Saathoff H, et al. (2012) Laser filament-induced aerosol formation. *Atmos Chem Phys Discuss* 12(11):29851–29885.
- Koop T, Luo BP, Tsias A, Peter T (2000) Water activity as the determinant for homogeneous ice nucleation in aqueous solutions. *Nature* 406(6796):611–614.
- Lindinger A, et al. (2004) Time-resolved explosion dynamics of H₂O droplets induced by femtosecond laser pulses. *Appl Opt* 43(27):5263–5269.
- Wilson CTR (1899) On the condensation nuclei produced in gases by the action of rontgen rays, uranium rays, ultra-violet light and other agents. *Philos Trans R Soc Lond A* 192:403–453.
- Rabeony H, Mirabel P (1987) Experimental study of vapor nucleation on ions. *J Phys Chem* 91(7):1815–1818.
- Wolk J, Strey R (2001) Homogeneous nucleation of H₂O and D₂O in comparison: The isotope effect. *J Phys Chem B* 105(47):11683–11701.
- Ladouceur HD, Baronavski AP, Lohrmann D, Grounds PW, Girardi PG (2001) Electrical conductivity of a femtosecond laser generated plasma channel in air. *Opt Commun* 189(1–3):107–111.
- Peter T, et al. (2006) Atmosphere. When dry air is too humid. *Science* 314(5804):1399–1402.
- Ebert V, Teichert H, Gieseemann C, Saathoff H, Schurath U (2005) Fiber-coupled in-situ laser absorption spectrometer for the selective detection of water vapour traces down to the ppb-level. *Technisches Messen* 72(1):23–30.